Corrosion of Carbon Steel in a Tropical Marine Environment Enhanced by H2S from Sargassum Seaweed Decomposition

Mahado Said Ahmed, Benoit Lescop, Julien Pellé, Stéphane Rioual, Christophe Roos, Mounim Lebrini

metals

MDPI

Article

Corrosion of Carbon Steel in a Tropical Marine Environment Enhanced by H_2S from *Sargassum* Seaweed Decomposition

Mahado Said Ahmed [1], Benoit Lescop [2], Julien Pellé [2], Stéphane Rioual [2], Christophe Roos [1] and Mounim Lebrini [1,*]

[1] Laboratoire des Matériaux et Molécules en Milieu Agressif UR 4_1, UFR STE, Université des Antilles, 97233 Schœlcher, Martinique, France; mahadosaidahmed@gmail.com (M.S.A.); christophe.roos@univ-antilles.fr (C.R.)

[2] Laboratoire des Sciences et Techniques de l'information de la Communication et de la Connaissance, CNRS, UMR 6285, Université de Brest, 29200 Brest, France; benoit.lescop@univ-brest.fr (B.L.); julien.pelle29@laposte.net (J.P.); stephane.rioual@univ-brest.fr (S.R.)

* Correspondence: mounim.lebrini@univ-antilles.fr; Tel.: +596-0596-72-74-42; Fax: +596-0596-28-47-86

Abstract: This article aims to investigate the atmospheric corrosion of carbon steel in a marine environment abundant in hydrogen sulfide (H_2S) resulting from the decomposition of *Sargassum* seaweed. To accomplish this, four sites with varying degrees of impact were chosen along the coast of Martinique. The corrosion rates of steel were evaluated through mass loss measurements. After one year of exposure, the corrosion rates were notably high, particularly in atmospheres rich in Cl^- ions and H_2S, ranging from 107 µm to 983 µm. Complementing these findings, surface and product morphologies were characterized using scanning electron microscopy (SEM) coupled with energy dispersive X-ray spectroscopy (EDS) and X-ray diffraction (XRD). These analyses revealed a significant degradation of the corrosion surface in the most affected atmospheres compared to those unaffected by *Sargassum* seaweed strandings. Lepidocrocite (γFeOOH) was identified as the predominant product regardless of the exposure atmosphere. However, goethite (αFeOOH) was found to be present in atmospheres most impacted by H_2S.

Keywords: atmospheric corrosion; *Sargassum* seaweed; carbon steel; H_2S; Cl^- ion; SEM/EDS; XRD

Citation: Said Ahmed, M.; Lescop, B.; Pellé, J.; Rioual, S.; Roos, C.; Lebrini, M. Corrosion of Carbon Steel in a Tropical Marine Environment Enhanced by H_2S from *Sargassum* Seaweed Decomposition. *Metals* **2024**, *14*, 676. https://doi.org/10.3390/met14060676

Academic Editor: Luis Cáceres

Received: 1 May 2024
Revised: 3 June 2024
Accepted: 5 June 2024
Published: 7 June 2024

1. Introduction

The topic of atmospheric corrosion of steel has been extensively researched and documented for a significant period [1–5]. The interest in this material stems from its essential role in various industries such as automotive manufacturing, construction, bridge building, mechanical engineering, and household appliances, owing to its economic and mechanical benefits such as ductility, formability, weldability, and strength [6]. The corrosion mechanism of steel is influenced by several environmental factors, including climatic conditions (humidity, temperature, etc.), the presence of atmospheric pollutants, as well as the exposure method and the surface condition of the material. Exposure to a marine atmosphere induces corrosion in steel, resulting in the development of a complex corrosion layer comprising oxides and oxyhydroxides. The proportions and morphological characteristics of this layer evolve over time with prolonged exposure. In the initial stages of corrosion, the presence of water on the steel surface triggers the formation of unstable iron II and III hydroxides, which subsequently transform into goethite (α-FeOOH) in the presence of sulfate ions or akaganeite (β-FeOOH) in the presence of chloride ions [7]. Additionally, lepidocrocite (γFeOOH) has been reported during the early stages [8].

Over the medium term, the corrosion layer can be divided into two successive sub-layers: (i) a dense, protective inner sub-layer primarily composed of goethite and maghemite [9] and (ii) an outer sub-layer containing lepidocrocite, goethite, and magnetite (Fe_3O_4) [10–12]. In the long term (approximately a century of exposure), the literature

mentions three types of corrosion surface morphology: (i) a single, relatively uniform layer; (ii) two sub-layers, with the internal layer mainly comprised of goethite, magnetite, maghemite (γ-Fe_2O_3), ferrihydrite ($Fe_2O_3 \cdot mH_2O$), or feroxyhyte (δ-FeOOH), and the external layer, which is more fissured, containing significant quantities of lepidocrocite and akaganeite [12]; and (iii) finally, in some samples, a third morphology is observed, which includes an outer "over-layer" containing impurities like quartz grains, in addition to the two aforementioned sub-layers.

For approximately a decade, the island of Martinique in the French West Indies has experienced significant occurrences of *Sargassum* seaweed strandings. Upon decomposition, these seaweeds emit substantial amounts of hydrogen sulfide (H_2S) into the atmosphere. Hydrogen sulfide is recognized as a potent oxidizing agent for various metals and metal alloys [13–15]. The anaerobic decomposition of stranded seaweed produces sulfides [16], a process similarly observed in sargassum accumulations. In these conditions, the growth of sulfate-reducing microorganisms under hypoxic or anoxic environments reduces sulfate compounds, releasing H_2S [17]. It is generally estimated that up to 50% of organic carbon in marine environments is mineralized through sulfate reduction under anaerobic conditions, leading to sulfide production [17]. Consequently, the decomposition of sargassum seaweed results in significant and effective H_2S formation. This new phenomenon makes steel corrosion more severe in an environment with a tropical climate (constant high temperatures (evaluated between 25 °C and 35 °C), high humidity, (75%) and high salinity) that is already conducive to corrosion. Recent studies have shown that atmospheric pollution linked to *Sargassum* seaweed has a strong impact on the corrosion of copper [18] and zinc [19]. This research revealed high corrosion rates for copper and zinc in the presence of *sargassum* algae, levels never reported before in the scientific literature. The corroded surfaces were primarily composed of CuS and ZnS. However, no study has yet been carried out on steel corrosion in marine atmospheric conditions rich in H_2S.

This study investigates the corrosion mechanisms of carbon steel in an uncontrolled tropical marine environment contaminated with H_2S from the decomposition of *sargassum* seaweed. The primary objective is to elucidate the specific role of the H_2S/Cl^- ion combination in this corrosion process. To achieve this, carbon steel samples were exposed to four distinct atmospheres with varying degrees of *sargassum* seaweed impact and consequent H_2S presence for a duration of one year. Corrosion progression was evaluated through mass loss measurements. Characterization of corrosion products was conducted using X-ray diffraction (XRD) and scanning electron microscopy (SEM) in conjunction with energy dispersive X-ray spectroscopy (EDS).

2. Materials and Methods

2.1. Selection of Sites

As mentioned earlier, the aim of this study is to investigate the corrosion of steel under conditions similar to those observed for copper and zinc [18,19]. The specific details of the four selected sites, as well as the concentrations of H_2S and chloride ions, have been detailed in these same previous publications [18,19]. The H_2S concentration monitoring device allows continuous, real-time measurement of H_2S concentrations. Data are transmitted remotely every ten minutes to a central database that consolidates all measurements taken by the network. Table 1 summarizes the annual average concentrations of H_2S and Cl^- ions recorded at the sites. In this regard, we will briefly mention the sites: Vert-Pré, Diamant, Frégate Est, and Vauclin. Based on these findings, we have identified four distinct types of exposure conditions:

- Type 1: A chloride-rich atmosphere with a minimal concentration of H_2S (Diamant);
- Type 2: A tropical atmosphere with low levels of both H_2S and chloride (Vert-Pré);
- Type 3: An atmosphere abundant in H_2S with minimal chloride concentration (Frégate Est);
- Type 4: An atmosphere abundant in H_2S (though less than type 3) and also containing high levels of Cl^- possibly at concentrations similar to type 1 (Vauclin).

Table 1. Average annual concentrations of H_2S and Cl^- ions in the different sites.

Site	H_2S (ppb)	Cl^- (mg m^{-2} day^{-1})
Diamant	7	481
Vert-Pré	15.5	46
Frégate Est	2995	60.5
Vauclin	223	

2.2. Preparation and Sample Exposure

Carbon steel DC01, whose chemical composition is provided in standard EN 10130/10139 (Table 2) [20,21], was utilized. The exposed samples measured 100 × 70 × 1 mm. Before exposure, all samples underwent mechanical polishing with SiC to grade 1200 to smoothen the surface and eliminate irregularities. Subsequently, they were rinsed with distilled water and ethanol, air-dried, and weighed to the nearest 10^{-4} g using an Adam Nimbus 210-001 microbalance (Grosseron company, Coueron, France). The samples were then subjected to outdoor atmospheric conditions on inclined desks at 45 °C in accordance with standard EN 13523-19 [22]. The maximum exposure duration was 12 months, with collection intervals every 3 months.

Table 2. Chemical composition of DC01 carbon steel.

Chemical Composition (%)			
C	**Mn**	***p***	**S**
≤0.12	≤0.60	≤0.045	≤0.045

2.3. Gravimetric Measurements

The steel samples, after exposure, were chemically treated in accordance with standard NF EN 8407 [23] to eliminate corrosion products. In this standard process, the samples were treated with a mixture of hydrochloric acid (500 mL) and hexamethylenetetramine (3.5 g) in distilled water to obtain 1000 mL, for 10 to 40 min at room temperature. Before any chemical treatment, the surfaces of the samples were mechanically brushed to remove any detached corrosion products. The treatment was carried out in an ultrasonic bath to optimize the process. This chemical cleaning process was repeated several times for each sample until a mass plateau was reached. The average corrosion rate was calculated from a triplicate sample.

2.4. Characterization and Identification of the Corrosion Product

The morphological and chemical analyses of the corrosion products were conducted by XRD and EDS/SEM following the procedures outlined in previous publications [18,19].

3. Results and Discussion

3.1. Assessment of Carbon Steel Thickness Loss after One-Year Exposure

The thickness loss was assessed through the measurement of mass loss to examine the corrosion behavior of carbon steel. These findings can aid in comparing corrosion processes documented in our locations with those observed elsewhere worldwide. Equation (1) was employed for calculating the thickness loss:

$$\varepsilon = \frac{\Delta m}{S \cdot d} \quad (1)$$

ε is the thickness loss (µm), Δm (g) is the mass difference between the initial mass and the mass after exposure and corrosion product removal, d is the density of the carbon steel (7.85 g·cm^{-3}), and S is the exposed area (cm^2).

Figure 1 shows the average carbon steel thickness losses as a function of exposure time at the four sites studied. The results for Diamant and Vert-Pré are shown in Figure 1a and those for Frégate Est and Vauclin in Figure 1b.

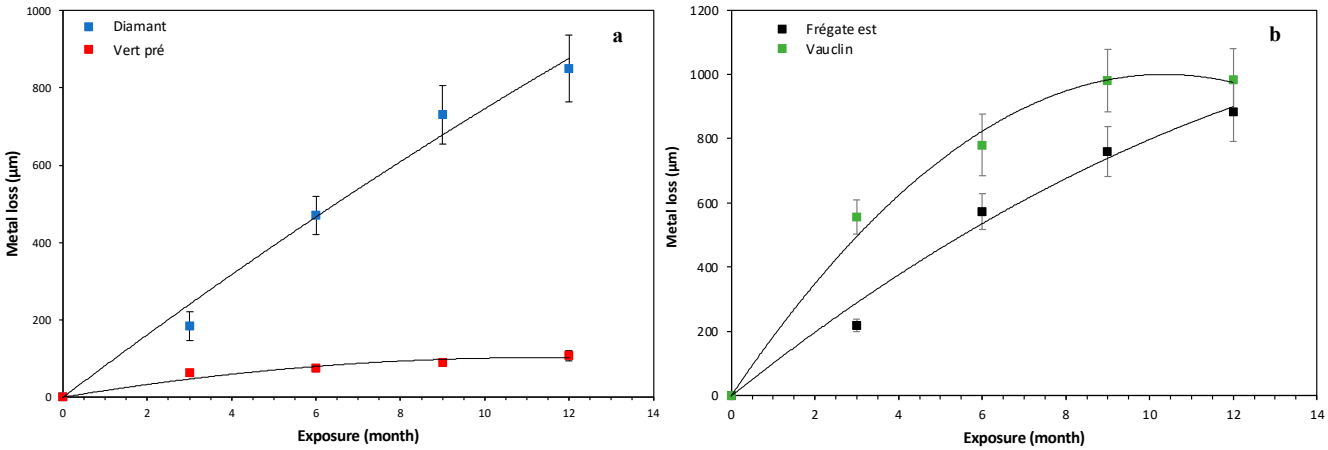

Figure 1. Thickness loss of carbon steel exposed in 4 sites: (**a**) Diamant and Vert-Pré, and (**b**) Frégate Est and Vauclin for 12 months.

The measured thickness losses of carbon steel after one year at Vert-Pré, Diamant, Frégate Est, and Vauclin stand at 107.2 µm, 850 µm, 883 µm, and 983 µm, respectively. These figures demonstrate a significant deviation from the corrosion rate data provided by the ISOCORROG [24], ICP/UNECE [25], and MICAT projects [26]. These projects aim to evaluate corrosion rates over one year across various sites in South America, Spain, and Portugal, encompassing diverse atmospheric conditions, including rural, marine, urban/industrial, and mixed. For carbon steel, the recorded corrosion rates typically fall within the range of 2.8 to 138 µm. The exceptional values observed in our study can be attributed to the unique combination of factors present, notably the presence of a marine atmosphere abundant in H_2S, along with Martinique's tropical climate and close proximity to the sea (ranging from a few meters to a few kilometers). The corrosion rates recorded at Diamant, Frégate Est, and Vauclin surpass the upper limits of class CX as defined by ISO 9223 [27], indicating extremely corrosive environmental conditions. It is worth noting that there are currently no comparable data available in the literature for marine atmospheres, highlighting the novelty and significance of our findings in this regard. Our experimental data were fitted by a prediction model involving a well-known logarithmic function [28–31]. In this model, the corrosion dynamic of carbon steel is described by the following Equation (2).

$$\varepsilon(t) = \varepsilon_{1year} \cdot t^n \quad (2)$$

In the equation provided, t represents the exposure time in years and constant ε_{1year} traditionally denotes the thickness lost after one year of exposure, while n serves as the exponent characterizing the protective efficacy of corrosion products. For all four sites, the n parameters are statistically significant at the 5% level, suggesting that exposure has a significant effect on metal loss. The models for Vauclin and Vert-Pré show that both parameters ε_{1year} and n are statistically significant. The calculated n values for the sites Frégate Est, Diamant, Vert-Pré, and Vauclin are 0.7181, 0.8300, 0.5162, and 0.3724, respectively. The values of n are all less than 1 for each site, indicating a sub-linear relationship between exposure and metal loss. This means that metal loss increases at a decreasing rate as exposure increases. According to Morcillo et al. [32], n values greater than 0.5 indicate the formation of a protective layer of corrosion products on the metal surface. Our experimental values are above 0.5, except for Vauclin, indicating the formation of a protective layer of corrosion products on the metal for the other sites. At Vauclin, the low value of n is linked to a decline in the corrosion rate attributed to significant dissolution of the steel after six months of exposure. The R^2 values for Frégate Est, Diamant, Vauclin,

and Vert-Pré are 0.9562, 0.9718, 0.9420, and 0.9619, respectively, indicating that the models fit the data reasonably well. This finding suggests that chloride (Cl^-) and hydrogen sulfide (H_2S) compounds exert significant influence on corrosion kinetics independently, while their combined presence results in considerably heightened damage. Furthermore, these results underscore that corrosion dynamics are predominantly influenced by the material itself, irrespective of the environmental conditions. It is noteworthy that no significant impact of seasonal variations on the corrosion kinetics is observed.

3.2. Characterization of Corrosion Products by SEM/EDS Analysis

For a comprehension of the carbon steel corrosion dynamics in the presence or absence of H_2S due to sargassum degradation, we conducted SEM/EDX measurements on the corroded surfaces. Figure 2 displays SEM images of the surfaces after exposure durations ranging from 3 to 12 months at four exposure sites.

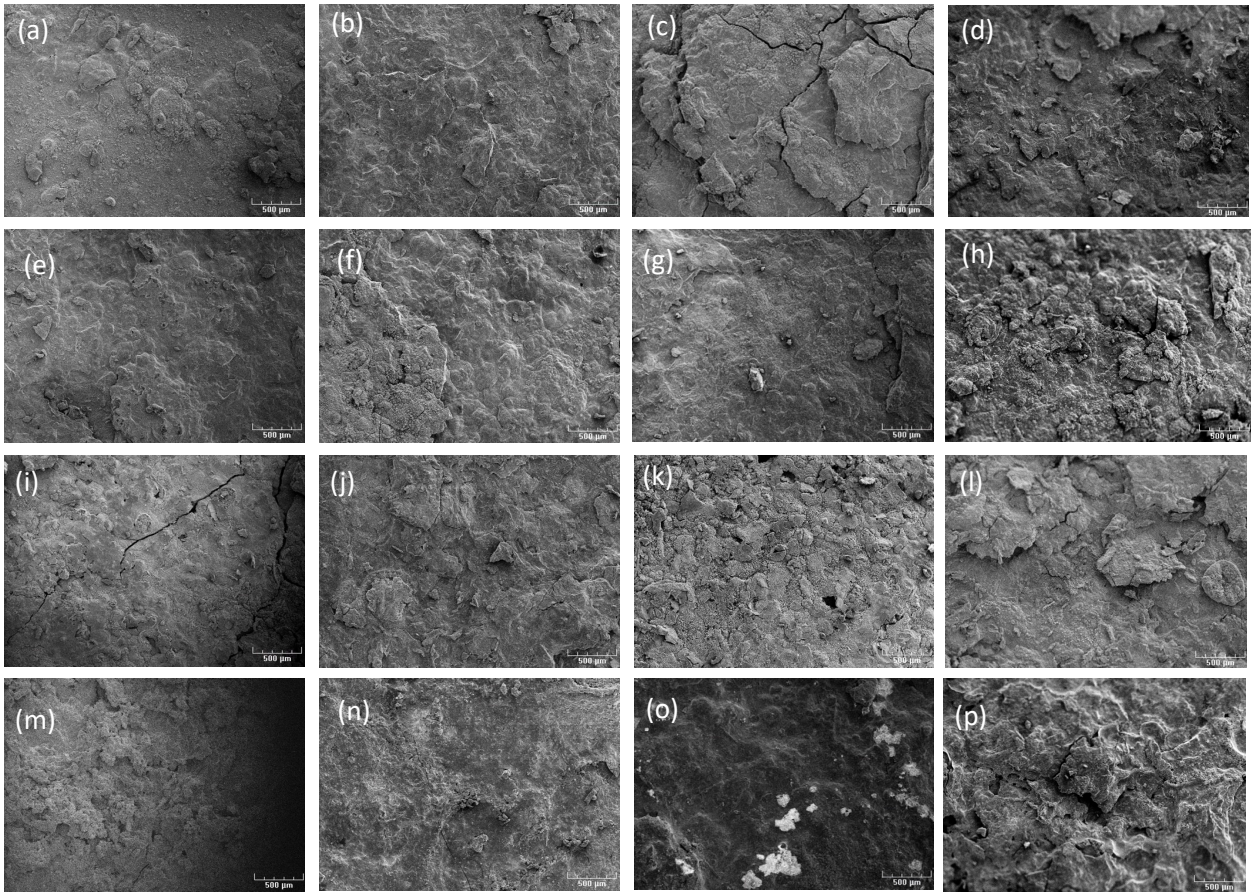

Figure 2. SEM images after 3, 6, 9, and 12 months of exposure in Vert-Pré (**a**–**d**), Diamant (**e**–**h**), Frégate Est (**i**–**l**), and Vauclin (**m**–**p**). The scale bar corresponds to 500 µm.

In Diamant and Vert-Pré, the observed surface morphologies typically resemble those commonly found in a marine atmosphere [33–35]. The evolution of the corrosion surface at these two sites is relatively similar. However, corrosion in Diamant appears to progress more rapidly. In fact, during the initial periods of exposure (3 to 6 months), the observed corrosion surface is irregular and granular, with the formation of clusters of corrosion products. Gradually, these clusters interconnect to form a compact layer. In the longer term, this second layer of corrosion cracks and flakes off. These different stages seem to repeat themselves over time. These morphological aspects can be explained by the consecutive formation of corrosion products of different natures and/or by the mechanical stresses intensifying within the thickening layer.

SEM images of the steel surfaces in Frégate Est and Vauclin display initially compact and highly rough structures (from the first months of exposure). With prolonged exposure, the corrosion surface experiences escalating stress, leading to the formation of cracks and detachment of the corrosion layer from the surface. Nevertheless, the metal substrate remains protected, indicating strong adherence of the inner layers to the metal surface. In contrast to the observations at the other two sites, the corrosion products formed appear to be uniform in nature and lack a protective effect on the surface. This rapid growth in the thickness of the corrosion products aligns with the gravimetric results. These observations are consistent with the aggressive nature of our pollutant-rich marine atmospheres.

In order to ascertain the elemental composition of the corrosion surface, EDS analyses were performed on surface areas measuring a few square millimeters. The quantitative analysis results following 1-year exposure are depicted in Table 3.

Table 3. EDS elemental composition in Vert-Pré, Diamant, Frégate Est, and Vauclin after 1 year of exposure (atomic percentage).

Site	Fe	O	Cl	S
Vert-Pré	20.3	79.2	0.3	0.2
Diamant	30.5	69.0	0.4	0.2
Frégate Est	28.2	64.5	/	7.3
Vauclin	20.8	77.3	1.1	0.8

In all sites, the predominant elements on the surface are iron and oxygen. This suggests that the corrosion products consist mainly of iron oxides and hydroxides. Chlorine levels are insignificant, even at a short distance from the sea, likely due to extensive leaching from the surface. The presence of trace amounts of sulfur can be attributed to the emission of H_2S after the sargassum has washed up and/or to aerosols containing sulfur from the sea. In Frégate Est and Vauclin, the presence of sulfur may indicate the formation of amorphous iron sulfide. However, sulfur levels are relatively moderate and show fluctuations over time. This could suggest an adsorption process of H_2S on the surface of the limited substrate. However, considering the corrosion rates measured at these sites, it is evident that the presence of this element, even in small quantities, significantly impacts the corrosion kinetics of the steel.

3.3. XRD Characterization of Corrosion Products

The surface corrosion products were also examined by XRD analysis. Figure 3 displays the diffractograms of DC01 steel samples exposed at the four sites for a duration of 12 months.

In Vert-Pré (Figure 3a) and Diamant (Figure 3b), lepidocrocite (γFeOOH) appears as the primary phase observed, accompanied by smaller quantities of magnetite (Fe_3O_4). Additionally, goethite (αFeOOH) is detected at the Vert-Pré site. These corrosion products have been previously identified in analogous marine environments [33–35]. The absence of chlorinated products is likely attributed to their solubility, unlike the stable basic salts observed with other metals.

To explain the process of formation and growth of the iron corrosion layer in a marine atmosphere, several mechanisms have been proposed in the literature [36–40]. These mechanisms lead to the formation of thermodynamically stable corrosion products through reactions such as hydrolysis, nucleation, crystallization, precipitation, dehydration, and dehydroxylation [41]. These reactions depend particularly on temperature, exposure time, and the pH of the surface.

In our case, the initially favorable process is the electrochemical oxidation of iron by dissolved O_2, as described by Equations (3) and (4).

$$Fe \rightarrow Fe^{2+} + 2e^{-} \quad (3)$$

$$O_2 + H_2O + 4e^- \rightarrow 2OH^- \quad (4)$$

$$Fe^{2+} + 2OH^- \rightarrow Fe(OH)_2 \quad (5)$$

In principle, the combination of these two half-equations forms iron (II) hydroxide, as described in Equation (5). However, the presence of atmospheric pollutants acidifies the electrolytic layer, inhibiting the formation of this product. Misawa et al. [39] suggest that under atmospheric corrosion conditions, various iron (II) hydroxo-complexes may form, depending on the anions present in the medium.

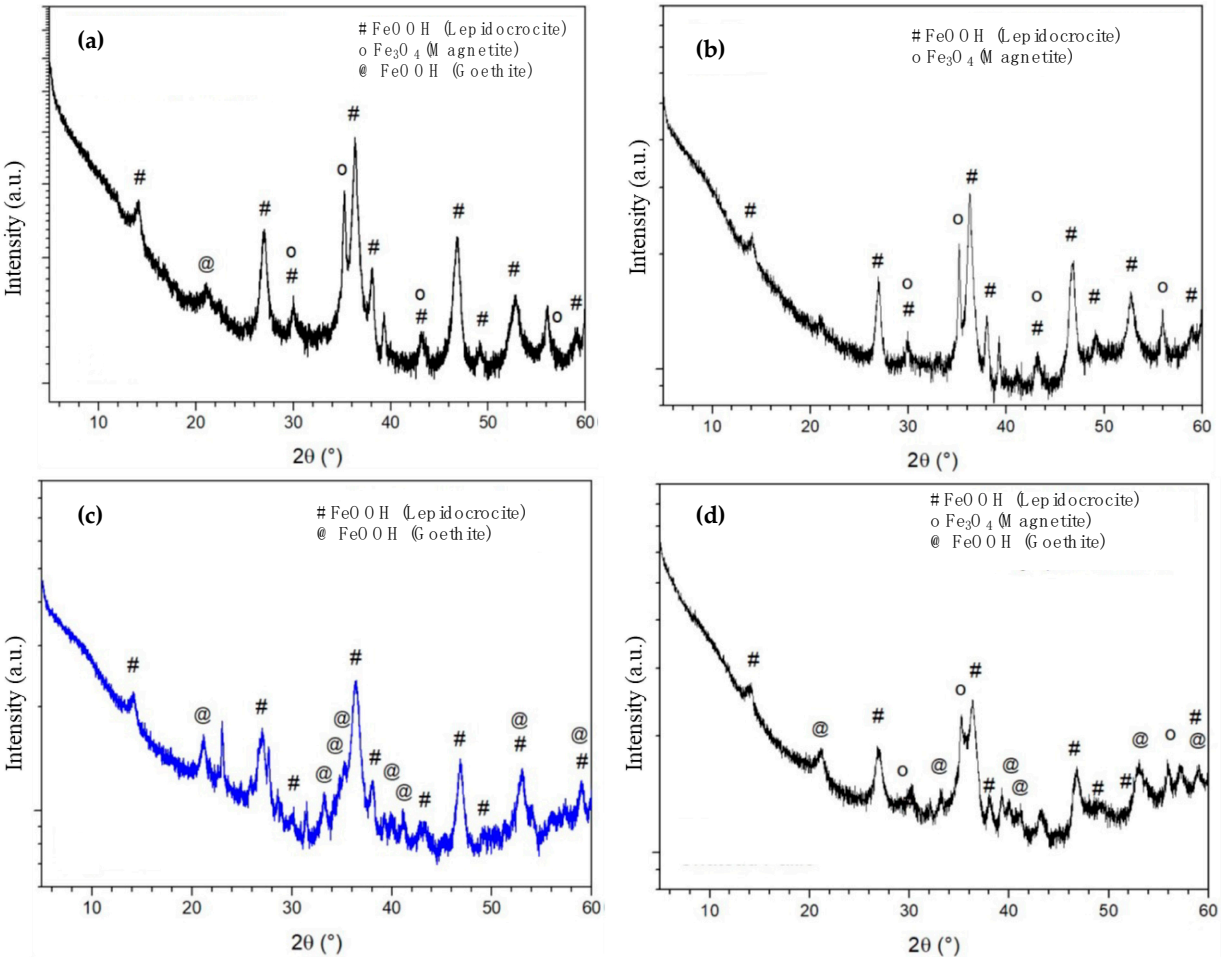

Figure 3. XRD diffractograms of DC01 carbon steel samples exposed 12 months in Vert-Pré (**a**), Diamant (**b**) Frégate Est (**c**) and Vauclin (**d**).

Lepidocrocite, which is predominantly present in the latter two sites, is the thermodynamically favored product due to the relatively low concentrations of Cl^- ions at the substrate surface [33]. The mechanism by which this product is formed is described in Equation (6) and involves two successive steps: hydrolysis of Fe^{2+} ions followed by oxidation and precipitation, resulting in the formation of $\alpha Fe(OH)^+$ hydroxo-complex. Alternating periods of humidity and drying accelerate this process of dissolution and precipitation.

$$Fe^{2+} \xrightarrow{\text{Hydrolysis}} Fe(OH)^+ \xrightarrow[\text{precipitation}]{\text{Oxidation}} \gamma FeOOH \quad (6)$$

Goethite is mainly detected in atmospheres farthest from the sea, which are therefore very low in Cl^- ions, typically like that of Vert-Pré. Ma et al. [42] proposed the formation of this compound in two steps from lepidocrocite and through the formation of an amorphous

ferric oxyhydroxide, as described in Equation (7). This process is favored during the drying cycle and releases HCl into the medium.

$$\gamma\text{FeOOH} \xrightarrow[\text{precipitation}]{\text{Chlorination}} \text{FeO}_x(\text{OH})_{2-2x}\text{Cl} \xrightarrow[\text{precipitation}]{\text{Solid state}} \alpha\text{FeOOH} + \text{HCl} \quad (7)$$

The increase in the thickness of the corrosion products over time leads to oxygen depletion in the inner layers and a reduction in the magnetite to lepidocrocite, as described by Equation (8) [43,44].

$$2 \quad \text{yFeOOH} + \text{Fe}^{2+} \rightarrow \text{Fe}_3\text{O}_4 + 2\text{H}^+ \quad (8)$$

Moreover, additional research [45,46] has demonstrated that, typically, magnetite can form through the reaction of ferric species originating from dissolved oxyhydroxides, in conjunction with ferrous species found in the electrolytic solution subsequent to the cathodic reaction, as represented by Equation (9).

$$\text{Fe}^{2+} + 8\text{FeOOH} + 2\text{e}^- \rightarrow 3\text{Fe}_3\text{O}_4 + 4\text{H}_2\text{O} \quad (9)$$

In Frégate Est, both goethite and lepidocrocite were observed to coexist after 12 months of exposure (see Figure 3c). However, lepidocrocite appears to predominate. In Vauclin, magnetite and goethite are the primary products, although lepidocrocite is also present (see Figure 3d). Despite the elevated concentrations of H_2S in the atmospheres at these sites, iron sulfide (FeS) was not detected via XRD analysis, in contrast to observations in submerged corrosion studies [47,48]. Several investigations have demonstrated the instability of iron sulfides at highly acidic pH levels [49]. The surface acidity in corrosion is induced by the sulfuric acid generated from H_2S oxidation, which also facilitates the transformation of lepidocrocite into goethite [33]. Consequently, in Vauclin, the elevated acidity and conductivity of the electrolytic solution accelerate the corrosion process. However, the presence of magnetite indicates that the acidity of the electrolytic solution is lower than that of Frégate Est, which is consistent with the higher H_2S concentrations measured in the latter site. According to Zittlau et al. [50], surface acidification is linked to the dissociation of H_2S. This is illustrated by Equations (10) and (11):

$$\text{H}_2\text{S} \rightarrow \text{H}^+ + \text{HS}^- \quad (10)$$

$$2\text{HS}^- \rightarrow 2\text{S}^{2-} + 2\text{H}^+ \quad (11)$$

4. Conclusions

This study investigated the impact of H_2S released from the degradation of *Sargassum* algae on the kinetics and morphology of carbon steel corrosion in four marine atmospheres in Martinique. The findings underscored the significant influence of the H_2S/Cl^- interaction on carbon steel corrosion. Specifically, corrosion rates were markedly higher in atmospheres with elevated concentrations of both H_2S and Cl^-. Conversely, atmospheres abundant in either H_2S or Cl^- exhibited comparable corrosion rates. Notably, the atmosphere distant from the *sargassum* beachings displayed a corrosion rate similar to that observed in typical marine environments. The corrosion products formed included lepidocrocite, goethite, and magnetite, commonly found in tropical atmospheres. However, their proportions varied depending on the atmospheric composition. Lepidocrocite predominated in Cl^--rich atmospheres, while goethite prevailed in H_2S-rich environments, attributed to the surface acidity induced by this compound. Collectively, these findings underscore the highly corrosive nature of Martinique's atmospheres.

Author Contributions: Conceptualization, M.L.; methodology, M.S.A., M.L., C.R., B.L. and S.R.; software, M.S.A.; validation, M.L.; formal analysis, M.S.A., M.L., B.L., S.R. and J.P.; investigation, M.S.A., M.L., B.L. and S.R.; resources, C.R.; data curation, M.S.A. and J.P.; writing—original draft

preparation, M.S.A., J.P. and M.L.; writing—review and editing, M.S.A. and M.L.; visualization, M.S.A. and M.L.; supervision, M.L.; project administration, M.L. and C.R.; funding acquisition, M.L. and C.R. All authors have read and agreed to the published version of the manuscript.

Funding: This research was funded by the Territorial Authority of Martinique (CTM) and the French National Research Agency (ANR); the project N° ANR-19-SARG-0006 (Impact des composes chimiques issus de la décomposition des sargasses et role des microorganismes sur la corrosion des matériaux métalliques. Considérations phénomélogique et juridique—CORSAiR).

Data Availability Statement: The raw data supporting the conclusions of this article will be made available by the authors on request.

Conflicts of Interest: The authors declare no conflicts of interest.

References

1. Evans, U.R. *The Corrosion and Oxidation of Metals: Scientific Principles and Practical Applications*; Edward Arnold Ltd.: London, UK, 1960.
2. Tomashov, N.D. *Theory of Corrosion and Protection of Metals. The Science of Corrosion*; The MacMillan Co.: New York, NY, USA, 1966.
3. Rozenfeld, I.L. *Atmospheric Corrosion of Metals*; NACE: Houston, TX, USA, 1972.
4. Feliu, S.; Morcillo, M.; Feliu, S., Jr. The prediction of atmospheric corrosion from meteorological and pollution parameters—II. Long-term forecasts. *Corros. Sci.* **2005**, *34*, 415–422. [CrossRef]
5. Leygraf, C.; Odnevall, W.; Tidblad, I. *Atmospheric Corrosion*, 2nd ed.; The Electrochemical Society Series; John Wiley and Sons: Hoboken, NJ, USA, 2016.
6. Béranger, G.; Henry, G.; Sanz, G. *Le livre de l'acier*; Lavoisier-Technique et Documentation: Paris, France, 1994.
7. Yamashita, M.; Konishi, H.; Kozakura, T.; Mizuki, J.; Uchida, H. In situ observation of initial rust formation process on carbon steel under Na_2SO_4 and NaCl solution films with wet/dry cycles using synchrotron radiation X-rays. *Corros. Sci.* **2005**, *47*, 2492–2498. [CrossRef]
8. Leidheiser, H.; Musić, S. The atmospheric corrosion of iron as studied by Mössbauer spectroscopy. *Corros. Sci.* **1982**, *22*, 1089–1096. [CrossRef]
9. Maréchal, L.; Perrin, S.; Dillmann, P.; Santarini, G. Experimental atmospheric ageing archaeological artefacts and contemporary low-alloy steel in climatic chamber. In Proceedings of the European Corrosion Congress, Lisbonne, Portugal, 4–8 September 2005.
10. Okada, H.; Hosoi, Y.; Yukawa, K.; Naito, H. Structure of the protective and decirative rust formed on low-alloy steels in the atmosphere. *Trans. ASM* **1969**, *62*, 278–281.
11. Keiser, J.T.; Brown, C.W.; Heidersbach, R.H. Characterization of the passive film formed on weathering steels. *Corros. Sci.* **1983**, *23*, 251–259. [CrossRef]
12. Bellot-Gurlet, L. Raman imaging of ancient trust scales on archaelogical iron artefacts for long term atmospheric corrosion mechanisms study. *J. Raman Spectrosc.* **2006**, *37*, 1228–1237.
13. Salas, B.V.; Wiener, M.S.; Badilla, G.L.; Beltran, M.C.; Zlatev, R.; Stoycheva, M.; Gaynor, J.T. *H_2S Pollution and Its Effect on Corrosion of Electronic Components, Air Quality-New Perspective*; IntechOpen: London, UK, 2012; pp. 263–285.
14. Becker, J.; Pellé, J.; Rioual, S.; Lescop, B.; Le Bozec, N.; Thierry, D. Atmospheric corrosion of silver, copper and nickel exposed to hydrogen sulphide: A multi-analytical investigation approach. *Corros. Sci.* **2022**, *209*, 110726. [CrossRef]
15. Rioual, S.; Lescop, B.; Pellé, J.; de Alkmim Radicchi, G.; Chaumat, G.; Bruni, M.D.; Becker, J.; Thierry, D. Development of low-cost RFID sensors dedicated to air pollution monitoring for preventive conservation. *Herit. Sci.* **2022**, *10*, 124. [CrossRef]
16. Foster, S.; Maher, W.; Schmeisser, E.; Taylor, A.; Krikowa, F.; Apte, S. Arsenic species in a rocky intertidal marine food chain in NSW, Australia, revisited. *Environ. Chem.* **2006**, *3*, 304–315. [CrossRef]
17. Bertrand, J.-C.; Doumenq, P.; Guyoneaud, R.; Marrot, B.; Martin-Laurent, F.; Matheron, R.; Moulin, P.; Soulas, G. Applied microbial ecology and decontamination—Micro-organisms that play a major role in the elimination of pollution that affects the environment. In *Microbial Ecology, Microbiology of Natural and Anthropogenic Environments*; Presses de l'Université de Pau et des Pays de l'Adour: Pau Cedex, France, 2011; pp. 705–798.
18. Said Ahmed, M.; Lebrini, M.; Lescop, B.; Pellé, J.; Rioual, S.; Amintas, O.; Boullanger, C.; Roos, C. Corrosion of Copper in a tropical marine atmosphere rich in H_2S Resulting from the decomposition of *Sargassum* algae. *Metals* **2023**, *13*, 982. [CrossRef]
19. Said Ahmed, M.; Lebrini, M.; Pellé, J.; Rioual, S.; Amintas, O.; Boullanger, C.; Lescop, B.; Roos, C. Study of atmospheric corrosion of zinc in a tropical marine environment rich in H_2S resulting from the decomposition of *sargassum* algae. *Mater. Corros.* **2024**, 1–9.
20. *EN 10130*; Cold rolled low carbon steel flat products for cold forming Technical delivery conditions. iTeh STANDARD PREVIEW: Brussels, Belgium, 2006.
21. *EN10139*; Cold rolled uncoated low carbon steel narrow strip cold forming—Technical delivery conditions. ILNAS: Brussels, Belgium, 2020.
22. *EN 13523-19*; Coil Coated Metals—Test Methods—Part 19: Panel Design and Method of Atmospheric Exposure Testing. iTeh Standard Preview: Brussels, Belgium, 2019.

23. *EN ISO-8407*; Removal of Corrosion Products from Corrosion Test Specimens. iTech Standard Preview: Rotkreuz, Switzerland, 2009.
24. Knotkova, D.; Kreislova, D.; Dean, W.S. *ISOCORRAG International Atmospheric Exposure Program: Summary of Results*; ASTM Data Serie 71; ASTM International: West Conshohocken, PA, USA, 2010; ISBN 978-0-8031-7011-7.
25. UNECE. *International Cooperative Programme on Effects on Materials Including Historic and Cultural Monuments*; Technical Manual, No. 1; Swedish Corrosion Institute: Gothenburg, Sweden, 1988.
26. Morcillo, M.; Almeida, E.; Rosales, B.; Uruchurtu, J.; Marrocos, M. *Corrosion y Protección de Metales en las Atmósferas de Iberoamérica. Parte I—Mapas de Iberoamérica de Corrosividad Atmosférica (Proyecto MICAT,XV.1/CYTED)*; CYTED: Madrid, Spain, 1998.
27. *ISO 9223:2012*; Corrosion of Metals and Alloys—Corrosivity of atmospheres—Classification, Determination and Estimation. iTech Standard Preview: Rotkreuz, Switzerland, 2012.
28. Belén, C.; De la Fuente, D.; Iván, D. Annual Atmospheric Corrosion of Carbon SteelWorldwide. An Integration of ISOCO RAGICP/UNECE and MICAT Databases. *Materials* **2017**, *10*, 601.
29. Panchenko, M.; Marshakov, A.; Igonin, T.N.; Kovtanyuk, V.V.; Nikolaeva, L.A. Long-term forecast of corrosion mass losses of technically important metals in various world regions using a power function. *Corros. Sci.* **2014**, *88*, 306–316. [CrossRef]
30. Rodríguez, J.J.S.; Hernández, F.J.S.; González, J.E. The effect of environmental and meteorological variables on atmospheric corrosion of carbon steel, copper, zinc and aluminium in a limited geographic zone with different types of environmen. *Corros. Sci.* **2003**, *45*, 799–815. [CrossRef]
31. Morcillo, M.; Chico, B.; Diaz, I.; Cano, H.; De la Fuente, D. Atmospheric corrosion data of weathering steels. *Corros. Sci.* **2013**, *77*, 6–24. [CrossRef]
32. Morcillo, M.; Feliu, S.; Simancas, J. Deviation from bilogarithmic law for atmospheric corrosion of steel. *Br. Corros. J.* **1993**, *28*, 50–52. [CrossRef]
33. Alcántara, J.; De la Fuente, D.; Chico, B. Marine Atmospheric Corrosion of Carbon Steel:A Review. *Materials* **2017**, *10*, 406. [CrossRef] [PubMed]
34. Seechurn, Y.; Wharton, J.A.; Surnam, B.Y.R. Mechanistic modelling of atmospheric corrosion of carbon steel in Port-Louis by electrochemical characterisation of rust layers. *Mater. Chem. Phys.* **2022**, *291*, 126694. [CrossRef]
35. Ma, Y.; Li, Y.; Wang, F. Corrosion of low carbon steel in atmospheric environments of different chloride content. *Corros. Sci.* **2009**, *51*, 997–1006. [CrossRef]
36. Rezel, D.; Genin, J.M.R. The substitution of chloride ions to OH^- ions in the akaganeite beta ferric oxyhydroxide studied by Mössbauer effect. *Hyperfine Interact* **1990**, *57*, 2067–2075. [CrossRef]
37. Feitknecht, W. The breakdown of oxide films on metal surfaces in acidic vapors and the mechanism of atmospheric corrosion. *Chimia* **1952**, *6*, 3–13.
38. Henriksen, J.F. Distribution of NaCl on Fe during atmospheric corrosionw. *Corros. Sci.* **1969**, *9*, 573–577. [CrossRef]
39. Misawa, T.; Kyuno, T.; Shimodaira, S. The mechanism of atmospheric rusting and the effect of Cu and P on the rust formation of low-alloy steels. *Corros. Sci.* **1971**, *11*, 35–48. [CrossRef]
40. Misawa, T.; Hashimoto, K.; Shimodaira, S. The mechanism of formation of iron oxide and oxyhydroxides in aqueous solutions at room temperature. *Corros. Sci.* **1974**, *14*, 131–149. [CrossRef]
41. Cornell, R.M.; Schwertmann, U. *The Iron Oxides: Structure, Properties, Reactions, Occurrences and Uses*, 2nd ed.; Wiley-VCH Verlag GmbH: Weinheim, Germany, 2003.
42. Ma, Y.; Li, Y.; Wang, F. The effect of β-FeOOH on the corrosion behavior of low carbon steel exposed in tropic marine environment. *Mater. Chem. Phys.* **2008**, *112*, 844–852. [CrossRef]
43. Schwarz, H. Über die Wirkung des magnetits beim atmosphärischen Rosten und beim Unterrosten von Anstrichen. *Mater. Corros.* **1972**, *23*, 648–663. [CrossRef]
44. Singh, A.K. Mössbauer and X-ray diffraction phase analysis of rusts from atmospheric test sites with different environments in Sweden. *Corros. Sci.* **1985**, *25*, 931–945. [CrossRef]
45. Ishikawa, T.; Kondo, Y.; Yasukawa, A.; Kandori, K. Formation of magnetite in the presence of ferric oxyhydroxides. *Corros. Sci.* **1998**, *40*, 1239–1251. [CrossRef]
46. Tanaka, H.; Mishima, R.; Hatanaka, N.; Ishikawa, T.; Nakayama, T. Formation of magnetite rust particles by reacting iron powder with artificial α-, β- and γ-FeOOH in aqueous media. *Corros. Sci.* **2014**, *78*, 384–387. [CrossRef]
47. Sun, W. *Kinetics of Iron Carbonate and Iron Sulfide Scale Formation in CO_2/H_2S Corrosion*; The Russ College of Engineering and Technology of Ohio University: Athens, OH, USA, 2006.
48. Cayard, M.S.; Maldonado, J.G. *Use and Misuse of Laboratory Tests*; NACE International: Orlando, FL, USA, 2000.
49. Ning, J.; Zheng, Y.; Young, D.; Brown, B.; Nesic, S. Thermodynamic Study of Hydrogen Sulfide Corrosion of Mild Steel. *Corrosion* **2014**, *70*, 335–389. [CrossRef]
50. Zittlau, A.H.; Shi, Q.; Boerio-Goates, J.; Woodfield, B.F.; Majzlan, J. Thermodynamics of the basic copper sulfate antlerite, posnjakite and brochantite. *Geochemistry* **2013**, *73*, 39–50. [CrossRef]